International Journal of Heat and Mass Transfer 68 (2014) 234–246

Contents lists available at ScienceDirect

International Journal of Heat and Mass Transfer

journal homepage: www.elsevier.com/locate/ijhmt

The onset of convection in a porous layer with multiple horizontal solid partitions

P.M. Patil [a,b], D.A.S. Rees [b,*]

[a] Department of Mathematics, JSS's Banashankari Arts, Commerce and Shanti Kumar Gubbi Science College, Vidyagiri, Dharwad 580 004, India
[b] Department of Mechanical Engineering, University of Bath, Bath BA2 7AY, UK

ARTICLE INFO

Article history:
Received 31 July 2013
Accepted 9 August 2013

Keywords:
Porous medium
Thermoconvective instability
Linear theory
Sublayers
Dispersion relation

ABSTRACT

The principal objective of the present paper is to investigate the onset of convection in a horizontal layer heated from below which consists of distinct porous sublayers which are separated by solid heat-conducting partitions. Each of the porous sublayers are identical as are the solid partitions. The present analysis employs linearised stability theory and a dispersion relation is derived from which neutral curves may be computed. For two-layer configurations the dispersion relation may be written explicitly, but for larger numbers of sublayers a simple systematic numerical procedure is used to compute the dispersion relation which, while it may also be written analytically, rapidly becomes increasingly lengthy as the number of sublayers increases. It is found that neutral curves are always unimodal and each has a well-defined single minimum. We attempt to give a comprehensive physical understanding of the effect of the number of layer, the relative thickness of the partitions and the conductivity ratio on the onset of convection and the form taken by the onset modes. Our results are compared with those of Rees and Genç (2011) [1] who considered the special case where the partitions are infinitesimally thin.

1. Introduction

A large number of papers have been published which have considered the effect of layering in one form or another on the onset and subsequent development of convection in layers heated from below. One of these, which considers two horizontal layers of fluid heated from below where the two fluid layers are separated by an impermeable horizontal interface, was written by Proctor and Jones [2]. A linear stability analysis yielded information about the onset of convection. It was found in some cases that the neutral stability curve is bimodal, and the authors then continued to consider weakly nonlinear convection where the two critical wavenumbers were in the ratio of 1:2. Catton and Lienhard V [3] considered a similar configuration but allowed the solid partition to be of finite thickness and therefore its conductivity became of importance.

In the present paper we also concentrate on a layer consisting of a number of sublayers, but attention is focussed on convection taking place in a porous medium rather than a clear fluid. The sublayers are identical in every respect and the partitions are also identical in every respect. Layering has been quite a favoured topic of study in the field of porous media because of its supposed application to geological systems. A series of papers by McKibbin and colleagues ([4–8] as well as others [9–11]) have teased out quite a substantial amount of information about the surprisingly detailed problem of the osnet of convection and its weakly nonlinear development. For a general layered system McKibbin and O'Sullivan [4] provided quite a comprehensive analysis of the onset problem and this was subsequently developed into a weakly nonlinear analysis by McKibbin and O'Sullivan [5]. A three-dimensional weakly nonlinear analysis by Rees and Riley [11] showed that two-dimensional convection is sometimes unstable, the realised pattern being a set of cells with square planform. They also found bimodal curves, which suggests that these may be quite ubiquitous in layered configurations. One example of a trimodal configuration was also found.

McKibbin and Tyvand [7] considered alternating configurations of sublayers, where neighbouring sublayers were thick and thin. The thermal properties of each type of sublayer were taken to be identical but the thin layers had low permeability. This meant that an anistropic modelling such as was undertaken in McKibbin and Tyvand [6] could not be done so easily because convection cells were found to be localised in the thick sublayers. Jang and Tsai [12] considered a three-layer configuration where the middle sublayer is impermeable, but thermally conducting, and of finite thickness. It was found that the system is at its most stable condition when the partition is located centrally. Rees and Genç [1] considered a variation on this overall theme by insisting that the thin layers were of infinitesimal thickness and impermeable. In such

* Corresponding author. Tel.: +44 1225 386775.
E-mail address: D.A.S.Rees@bath.ac.uk (D.A.S. Rees).

0017-9310/$ - see front matter © 2013 Published by Elsevier Ltd.
http://dx.doi.org/10.1016/j.ijheatmasstransfer.2013.08.029

Nomenclature

A, B, C, D	constants
A^*, B^*	constants
CHF	constant heat flux
CT	constant temperature
d	conductivity ratio
$\underline{d}$	vector defined in (30)
g	gravity
h	height of the solid partitions
H	height of the porous sublayers
$\mathcal{H}$	height of the compsite layer
k	disturbance wavenumber
k_s	thermal conductivity of solid
k_{pm}	thermal conductivity of porous medium
K	permeability
$\mathcal{M}, \mathcal{N}$	4×4 matrices
N	number of porous sublayers
p	pressure
Ra	Darcy–Rayleigh number
t	time
T	temperature of solid
$\mathcal{T}$	disturbance in T
u	horizontal velocity
$\underline{v}$	vector of coefficients
w	vertical velocity
x	horizontal coordinate
z	vertical coordinate

Greek symbols

α	thermal diffusivity
β	thermal expansion coefficient
γ	constant
δ	thickness ratio
ΔT	temperature scaled
θ	temperature of porous medium
Θ	disturbance in θ
κ	diffusivity ratio
λ	constant
μ	dynamic viscosity
ρ	density
σ	constant
ψ	streamfunction
Ψ	disturbance streamfunction

Subscripts and superscripts

c	cold boundary
h	hot boundary
j	sublayer index
pm	porous medium
s	solid phase
$'$	derivative with respect to z
1,2,...	sublayer indices

composite layers convection patterns are localised within the porous sublayers. There were three surprising results which were found: (i) neutral curves naturally bunch into groups of N when there are N sublayers; (ii) the dispersion relation for N sublayers factorises into N similar factors, and this facilitates a large part of the general analysis while explaining the bunching of the neutral curves, and (iii) the system tends towards one with a critical Rayleigh number of 12 and wavenumber of 0 as the number of sublayers increases — this is significant because these critical values correspond to a single porous layer subject to constant heat flux boundary conditions, whereas the overall problem has constant temperature boundary conditions.

In this paper we consider a more physically realistic version of the work undertaken by Rees and Genç [1]. The porous layer will consist of N identical porous sublayers, which are separated by identical solid partitions, but these partitions have finite thickness. A formula for the dispersion relation is obtained, account being taken of the temperature variations within the solid partitions. We obtain neutral curves, mode shapes and the manner of the variation in the critical values as the governing parameters (namely the diffusivity ratio, d, the thickness ratio, δ, and the number of porous sublayers, N) vary.

2. Governing equations

We consider the onset of convection in a horizontal porous layer which consists of a number of identical porous sublayers of thickness, H, which are separated by solid partitions each of thickness, h. Thus while fluid may not pass from one sublayer to another, conductive heat transfer may take place through the solid partitions. A configuration which consists of three sublayers is depicted in Fig. 1.

It is assumed that the Boussinesq approximation is valid, that the porous medium is homogeneous and isotropic, that the phases are in local thermal equilibrium, and that the fluid motion satisfies Darcy's law in addition to the buoyancy effects. Given the above dimensions, a general system of N porous sublayers has overall height, $\mathcal{H}$, given by

$$\mathcal{H} = NH + (N-1)h. \tag{1}$$

Dirichlet boundary conditions for temperature are applied on the outer horizontal surfaces of the layer, as shown in Fig. 1, and the continuity of both temperature and heat flux conditions are applied at all interfaces. The governing equations are non-dimensionalised by using H as the representative lengthscale, rather than $\mathcal{H}$, and by using the temperature drop across one sublayer, rather than across the system as whole; this has the advantage of yielding much easier comparisons between cases which consist of different numbers of sublayers, particularly the classical single-layer Darcy–Bénard problem. Given that we are performing a linear stability analysis in an unbounded horizontal layer, all three-dimensional modes may be decomposed into sums or integrals of two-dimensional roll cells. Here, we present our analysis in terms of two-dimensional equations. The non-dimensional governing equations for the problem considered herein are given by (see [13]),

$$\frac{\partial u_j}{\partial x} + \frac{\partial w_j}{\partial z} = 0, \tag{2}$$

$$u_j = -\frac{\partial p_j}{\partial x}, \tag{3}$$

$$w_j = -\frac{\partial p_j}{\partial z} + Ra\ \theta_j, \tag{4}$$

$$\frac{\partial \theta_j}{\partial t} + u_j \frac{\partial \theta_j}{\partial x} + w_j \frac{\partial \theta_j}{\partial z} = \frac{\partial^2 \theta_j}{\partial x^2} + \frac{\partial^2 \theta_j}{\partial z^2} \tag{5}$$

for porous sublayer j, where $1 \leqslant j \leqslant N$, and by

$$\frac{\partial T_j}{\partial t} = \kappa \left(\frac{\partial^2 T_j}{\partial x^2} + \frac{\partial^2 T_j}{\partial z^2} \right) \tag{6}$$

for solid layer, j where $1 \leqslant j \leqslant N-1$, and where κ is the diffusivity ratio, α_s/α_{pm}. In the above, Ra is the Darcy–Rayleigh number which is defined according by

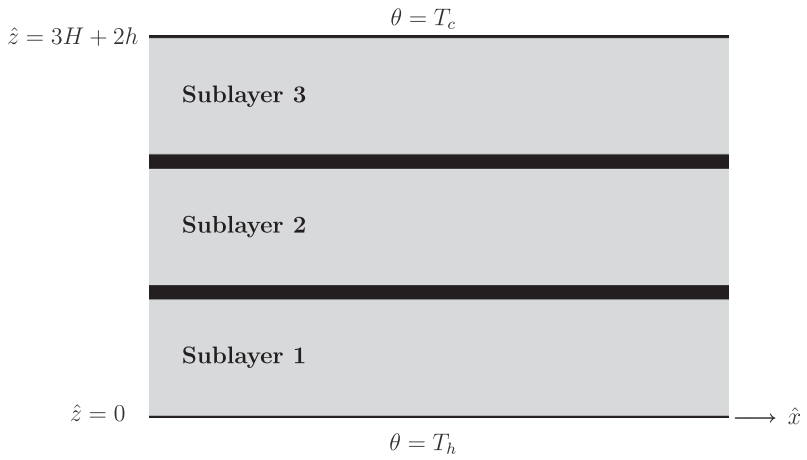

Fig. 1. Definition sketch for the problem being solved. Showing a system consisting of three identical porous sublayers (grey) each of height, H, with two identical solid partitions (black) each of height, h.

$$Ra = \frac{\rho g \beta H K \Delta T}{\mu \alpha_{\rm pm}}. \tag{7}$$

We note that, if the upper and lower surfaces of the composite layer are maintained at the respective dimensional temperatures of T_c and T_h, then ΔT, which is the temperature drop across one porous sublayer, is given by,

$$T_h - T_c = \Delta T\left[N + (N-1)\frac{k_{\rm pm} h}{k_s H}\right]. \tag{8}$$

Therefore, if we had used the thickness and temperature drop across the full layer in the definition of the Darcy–Rayleigh number, then it would be larger by the factor,

$$\left[N + (N-1)\frac{k_{\rm pm} h}{k_s H}\right]\left[N + (N-1)\frac{h}{H}\right], \tag{9}$$

than the present definition.

Without loss of generality we restrict our analysis to two dimensions and therefore the streamfunction, ψ, may be introduced for the porous sublayers as follows,

$$u_j = -\frac{\partial \psi_j}{\partial z}, \quad w_j = \frac{\partial \psi_j}{\partial x}. \tag{10}$$

Therefore Eq. (2) is satisfied, while Eqs. (3)–(5) reduce to,

$$\frac{\partial^2 \psi_j}{\partial x^2} + \frac{\partial^2 \psi_j}{\partial z^2} = Ra\ \frac{\partial \theta_j}{\partial x}, \tag{11}$$

$$\frac{\partial \theta_j}{\partial t} + \frac{\partial \psi_j}{\partial x}\frac{\partial \theta_j}{\partial z} - \frac{\partial \psi_j}{\partial z}\frac{\partial \theta_j}{\partial x} = \frac{\partial^2 \theta_j}{\partial x^2} + \frac{\partial^2 \theta_j}{\partial z^2}. \tag{12}$$

These equations are to be solved subject to the following boundary and interface conditions,

$$\begin{aligned}
&z = 0: \ \psi_1 = 0, \quad \theta_1 = N + (N-1)\delta/d,\\
&z = j + (j-1)\delta: \ \psi_j = 0, \quad \theta_j = T_j, \quad k_{\rm pm}\frac{\partial \theta_j}{\partial z} = k_s \frac{\partial T_j}{\partial z},\\
&z = j + j\delta: \ \psi_j = 0, \quad \theta_{j+1} = T_j, \quad k_{\rm pm}\frac{\partial \theta_{j+1}}{\partial z} = k_s \frac{\partial T_j}{\partial z},\\
&z = N + (N-1)\delta: \psi_N = 0, \quad \theta_N = 0,
\end{aligned} \tag{13}$$

where $j = 1, \ldots, N-2$.

This problem may now be seen to depend on four nondimensional parameters: N, the number of porous sublayers, $\delta = h/H$, the thickness of the solid sublayers relative to the porous sublayers, κ, the thermal diffusivity ratio, and $d = k_s/k_{\rm pm}$, the thermal conductivity ratio. We note that the analysis of Rees and Genç [1] corresponds to the case, $\delta = 0$, where the solid layers are infinitesimally thin. Given that the onset of convection may be shown to be stationary (i.e. there is no Hopf bifurcation) these four parameters may be reduced to three (δ, d, and N) since κ multiplies a time-derivative term.

3. Linear stability analysis

3.1. Perturbation equations

The basic state which we analyse for stability is one for which there is no flow, and there is a temperature profile which is piecewise linear:

$$\psi_j = 0, \qquad \frac{\partial \theta_j}{\partial z} = -1, \quad \frac{\partial T_j}{\partial z} = -\frac{1}{d}, \tag{14}$$

where $j = 1, \ldots N$ for the porous sublayers, and $j = 1, \ldots N-1$ for the solid partitions. Perturbations are introduced by means of the substitutions,

$$\begin{aligned}
&\psi_j(x,z) = \Psi_j(z)\cos kx, \quad \theta_j(x,z) = \Theta_j(z)\sin kx,\\
&T_j(x,z) = \mathcal{T}_j(z)\sin kx,
\end{aligned} \tag{15}$$

where the disturbances are assumed to be sufficiently small that products of the disturbances may be neglected. Here the value, k, is the wavenumber. The governing equations for the disturbances are,

$$\Psi_j'' - k^2 \Psi_j = k\ Ra\ \Theta_j', \tag{16}$$

$$\Theta_j'' - k^2 \Theta_j = k\ \Psi_j', \tag{17}$$

$$\mathcal{T}_j'' - k^2 \mathcal{T}_j = 0 \tag{18}$$

and the boundary and interface conditions become,

$$\begin{aligned}
&z = 0: \ \Psi_1 = 0, \quad \Theta_1 = 0,\\
&z = j + (j-1)\delta: \ \Psi_j = 0, \quad \Theta_j = \mathcal{T}_j, \quad \frac{\partial \theta_j}{\partial z} = d\frac{\partial \mathcal{T}_j}{\partial z},\\
&z = j + j\delta: \ \Psi_j = 0, \quad \Theta_{j+1} = \mathcal{T}_j, \quad \frac{\partial \theta_{j+1}}{\partial z} = d\frac{\partial \mathcal{T}_j}{\partial z},\\
&z = N + (N-1)\delta: \Psi_N = 0, \quad \Theta_N = 0.
\end{aligned} \tag{19}$$

Eqs. (16)–(19) now form an eigenvalue problem for the Darcy–Rayleigh number as a function of the wavenumber, k, and the three governing parameters, namely δ, d and N. These equations may be solved numerically by introducing suitable modifications to codes which employ the shooting method, for example. However, it

proves very much simpler and very much quicker to write a short code which computes a dispersion relation.

3.2. Derivation of the dispersion relation

Eqs. (16)–(19) take the form of a linear constant-coefficient system and therefore all possible solutions take the form, $e^{\alpha z}$, where α may be either real or complex. The solution of these equations in porous sublayer 1 may be written in the form,

$$\begin{aligned}\Psi_1 &= Ra^{1/2}[A_1\sinh\lambda z + B_1\cosh\lambda z + C_1\sin\sigma z + D_1\cos\sigma z],\\ \Theta_1 &= A_1\sinh\lambda z + B_1\cosh\lambda z - C_1\sin\sigma z - D_1\cos\sigma z,\end{aligned} \tag{20}$$

where

$$\lambda = (k\,Ra + k^2)^{1/2} \quad \text{and} \quad \sigma = (k\,Ra - k^2)^{1/2}. \tag{21}$$

We may apply the boundary conditions, $\Psi_1(0) = 0$, $\Psi_1(1) = 0$, and $\Theta_1(0)$ to obtain $B_1 = D_1 = 0$ and the relation, $A_1\sinh\lambda + C_1\sin\sigma = 0$.

If we were to consider just one porous layer with no intermediate solid partitions, then the application of the final boundary condition, $\Theta_1(1) = 0$, leads either to $A_1\sin\lambda = 0$ or to $C_1\sin\sigma = 0$. The former may be solved only by setting $A_1 = 0$. The latter is satisfied when $\sin\sigma = 0$, and the definition of σ given above leads quickly to the usual expression for the Darcy–Rayleigh number in terms of the wavenumber:

$$Ra = \frac{(k^2 + n^2\pi^2)^2}{k^2}, \tag{22}$$

where n denotes the mode number. The lowest critical value of Ra arises when $n = 1$, and it corresponds to $k_c = \pi$ and $Ra_c = 4\pi^2$ after minimisation of Ra with respect to k.

When we consider more than one porous sublayer, then we note first that the vector of the coefficients for the lowest porous sublayer which were introduced in Eq. (20) may be written in the form,

$$\underline{v}_1 = \begin{pmatrix} A_1\\ B_1\\ C_1\\ D_1\end{pmatrix} = \begin{pmatrix} \sin\sigma\\ 0\\ -\sinh\lambda\\ 0\end{pmatrix}. \tag{23}$$

The solution of Eq. (18) for $\mathcal{T}_1$ in the first solid partition ($j = 1$) is now,

$$\mathcal{T}_1 = A_1^*\sinh k(z-1) + B_1^*\cosh k(z-1), \tag{24}$$

where

$$\begin{aligned}A_1^* &= [\lambda A_1\cosh\lambda + \lambda B_1\sinh\lambda - \sigma C_1\cos\sigma + \sigma D_1\sin\sigma]/kd,\\ B_1^* &= A_1\sinh\lambda + B_1\cosh\lambda - C_1\sin\sigma - D_1\cos\sigma.\end{aligned} \tag{25}$$

Having the solution for $\mathcal{T}_1$, it is now possible to use the appropriate boundary and interface conditions to relate the solutions in porous sublayer 1 to those in porous sublayer 2. Given that the porous sublayers are identical, and that the solid partitions are also identical, it means that we may write down the following expression relating the respective vectors of coefficients for porous sublayers $j+1$ and j:

$$\begin{pmatrix} 0 & 1 & 0 & 1\\ \sinh\lambda & \cosh\lambda & \sin\sigma & \cos\sigma\\ 0 & 1 & 0 & -1\\ \lambda & 0 & -\sigma & 0\end{pmatrix}\begin{pmatrix} A_{j+1}\\ B_{j+1}\\ C_{j+1}\\ D_{j+1}\end{pmatrix} = \begin{pmatrix} 0 & 0 & 0 & 0\\ 0 & 0 & 0 & 0\\ (\lambda/kd)\sinh\delta k\cosh\lambda + \cosh\delta k\sinh\lambda & (\lambda/kd)\sinh\delta k\sinh\lambda + \cosh\delta k\cosh\lambda & -(\sigma/kd)\sinh\delta k\cos\sigma - \cosh\delta k\sin\sigma & (\sigma/kd)\sinh\delta k\sin\sigma - \cosh\delta k\cos\sigma\\ \lambda\cosh\delta k\cosh\lambda + kd\sinh\delta k\sinh\lambda & \lambda\cosh\delta k\sinh\lambda + kd\sinh\delta k\cosh\lambda & -\sigma\cosh\delta k\cos\sigma - kd\sinh\delta k\sin\sigma & \sigma\cosh\delta k\sin\sigma - kd\sinh\delta k\cos\sigma\end{pmatrix}\begin{pmatrix} A_j\\ B_j\\ C_j\\ D_j\end{pmatrix}, \tag{26}$$

where

$$\begin{aligned}\Psi_j &= Ra^{1/2}[A_j\sinh\lambda z + B_j\cosh\lambda z + C_j\sin\sigma z + D_j\cos\sigma z],\\ \Theta_j &= A_j\sinh\lambda z + B_j\cosh\lambda z - C_j\sin\sigma z - D_j\cos\sigma z,\end{aligned} \tag{27}$$

for $j = 1,\ldots,N$. Eq. (26) may be written in more compact form as

$$\mathcal{M}\underline{v}_{j+1} = \mathcal{N}\underline{v}_j. \tag{28}$$

Hence it is possible to solve for $\underline{v}_{j+1}$ in terms of $\underline{v}_j$, where $\underline{v}_1$ is given by Eq. (23). The solution procedure is completed by the application of the final boundary condition, namely that

$$\Theta_N(N + (N-1)\delta) = 0 \Rightarrow A_N\sinh\lambda + B_N\cosh\lambda - C_N\sin\sigma - D_N\cos\sigma = 0. \tag{29}$$

If we now define

$$\underline{d} = (\sinh\lambda, \cosh\lambda, -\sin\sigma, -\cos\sigma), \tag{30}$$

then the application of this boundary condition yields the following general expression for the required dispersion relation:

$$\underline{d}.\underline{v}_N = 0 \Rightarrow \underline{d}.\left[(\mathcal{M}^{-1}\mathcal{N})^{N-1}\right]\cdot\underline{v}_1 = 0. \tag{31}$$

This is a relatively simple formula to encode, and the task is made even simpler when one recognizes that the inversion of $\mathcal{M}$ may be replaced by the inversion of two 2×2 matrices instead. In general it is impossible to solve the resulting formula explicitly for Ra in terms of k, but numerical solution may be found using a simple Newton–Raphson formula. Neutral curves are most easily plotted by simply evaluating the formula for the dispersion relation on a fine grid of values of Ra and k and then drawing the zero contours; this procedure guarantees that no isolated branches of the neutral curve are omitted. Critical points are evaluated using a different Newton–Raphson scheme, one which has been described in detail in other papers; see Rees and Genç [1] and Rees and Mojtabi [14].

While it is possible in principle to expand the dispersion relation given in Eq. (31), the resulting formulae are exceptionally lengthy to write down. However, when $N = 2$, we find that the dispersion relation takes the following form:

$$\begin{aligned}&4kd\cosh\delta k\sinh\lambda\sin\sigma(\lambda\cosh\lambda\sin\sigma + \sigma\sinh\lambda\cos\sigma)\\ &\quad + \sinh\delta k[(\lambda\cosh\lambda\sin\sigma + \sigma\sinh\lambda\cos\sigma)^2\\ &\quad + (2kd\sinh\lambda\sin\sigma)^2] = 0.\end{aligned} \tag{32}$$

From this expression we see that the limit, $\delta \to 0$ (infinitesimally thin solid partitions), yields

$$\sin\sigma(\lambda\cosh\lambda\sin\sigma + \sigma\sinh\lambda\cos\sigma) = 0, \tag{33}$$

which was derived in Rees and Genç [1].

4. Results and discussion

Our aim here is to provide a sufficient amount of information for a general understanding to be gained of the general properties of the onset problem for a layered porous system with conducting interfaces. This will include how neutral curves and mode shapes vary with the main nondimensional parameters, d and δ, and with N, the number of sublayers. To this end it will also be necessary to consider higher modes. A comprehensive account of the onset problem will be given for a selection of values of N, together with some general properties of mode shapes and the variation in critical values as the governing parameters vary. Many of the properties of such layered systems will be explained by comparison with the three main instances of the classical Darcy–Bénard problem with impermeable boundaries. There are three possible combinations of constant temperature and constant heat flux surfaces which may be considered; the relevant onset criteria for the single-layer problem are given in Table 1.

Table 1
Critical values of Ra and k for different combinations of constant temperature (CT) and constant heat flux (CHF) surfaces.

	Ra_c	k_c
CT/CT	$4\pi^2$	π
CT/CHF	27.097628	2.326214
CHF/CHF	12	0

4.1. Neutral curves and mode shapes

Some representative neutral curves are shown in Fig. 2 for two, three, four and five layers, while some corresponding mode shapes are displayed in Fig. 3. In each case we have selected the solid partitions to have a nondimensional thickness of $\delta = 0.1$. In each subfigure in Fig. 2 we show the first N modes for each of the cases, $d = 0.1$, 1 and 10, where there are N porous sublayers. Each of these curves possess a single minimum, and an extensive survey of a

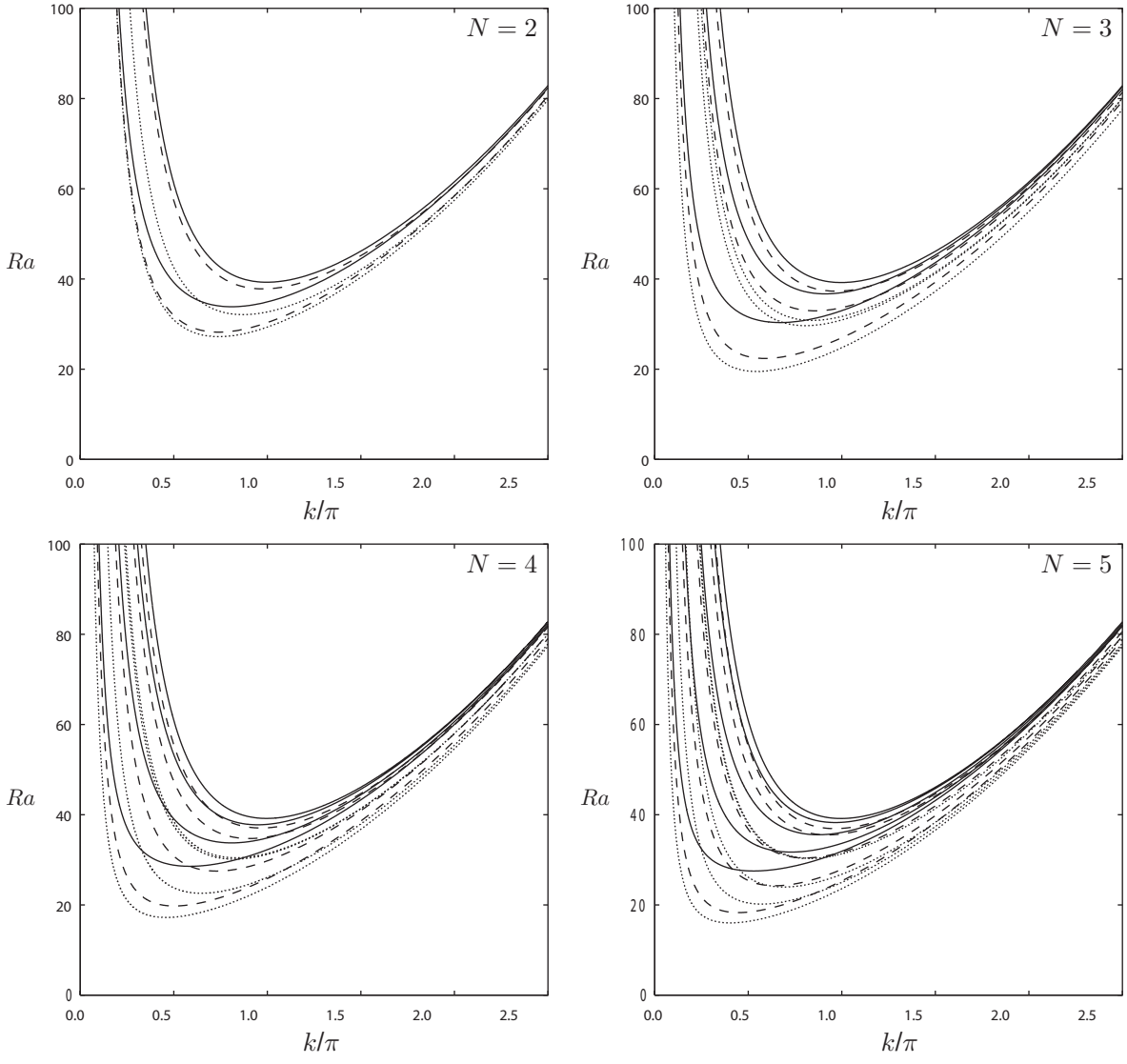

Fig. 2. Neutral curves for the first N modes for $N = 2$, 3, 4 and 5, and for $\delta = 10$. Continuous lines correspond to $d = 10$, dashed lines to $d = 1$ and dotted lines to $d = 0.1$.

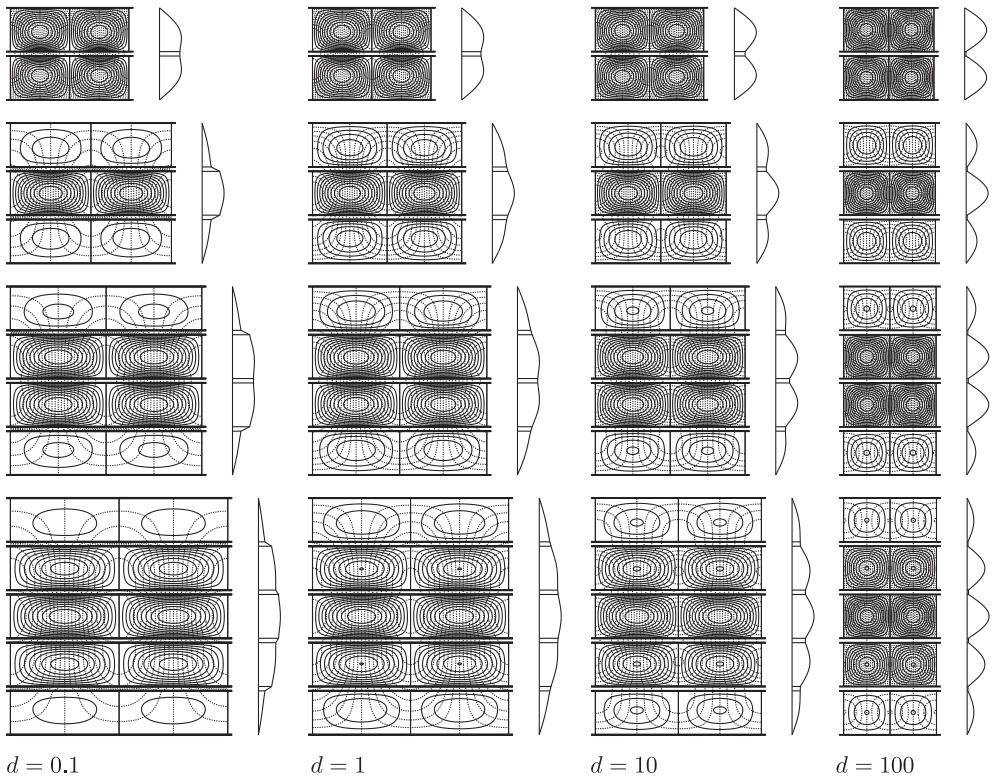

Fig. 3. Profiles of the most unstable disturbance for $\delta = 0.1$ with $d = 0.1$, 1, 10 and 100, and for $N = 2$, 3, 4 and 5. Continuous lines correspond to streamlines and dotted lines to isotherms. The aspect ratio of each case represents faithfully the most unstable wavenumber. The vertical profile of the temperature disturbance is given to the right of each set of isolines.

wide range of parameters seems to suggest that this is a univeral property of such convecting systems. However, we note that other types of layered system such those considered by Proctor and Jones [2] and Rees and Riley [11], in which the sublayers may have different thickness and physical properties, admit neutral curves with more than one minimum in certain ranges of the governing parameters.

For each value of N we find that the critical Rayleigh number (i.e. the minimum value) and its associated wavenumber decreases as the conductivity ratio, d, decreases. The reason for this may be understood to some extent by appealing to the effective boundary conditions at the interfaces between the solid partitions and the porous sublayers. Therefore when d takes decreasing values the partitions have a decreasing conductivity, and therefore internal porous sublayers (i.e. for cases where $N \geqslant 3$) have boundary conditions which tend to approximate increasingly well to the CHF/CHF case shown in Table 1. Thus decreasing values of d cause the critical values of Ra and d to decrease. When $N = 2$ similar arguments may be made, although the sublayers now tend towards the CT/CHF case given in Table 1 when d decreases and the critical values when $d = 0.1$ are close to those given in Table 1.

On the other hand, when d is very large compared with unity, the solid partitions are highly conducting, and therefore internal sublayers have boundary conditions which approximate to the CT/CT case shown in Table 1. Therefore the critical values of Ra and k rise and are closer to $4\pi^2$ and π, respectively. However, the situation is not as straightforward as this simple explanation suggests. The critical values when $d = 10$ which are shown in Fig. 2 are much closer to the data given in [1], than to the CT/CT cases. One reason for this is that, while the streamlines show that the flow consists of a stack of co-rotating cells, the temperature profile is essentially unicellular. But this aspect will be returned to later in the paper.

Although we do not show this explicitly due to lack of space, the layers considered here have neutral curves which obey the same 'clumping' properties as were given in [1]. Thus a system composed of N porous sublayers finds the neutral curves bunching into separate groups of N curves as k becomes large. We will not analyse this feature mathematically because the dispersion relation derived here does not lend itself to the simple factorisation found in [1], who considered the case $\delta = 0$.

Fig. 3 shows some mode shapes corresponding the critical Rayleigh numbers for $N = 2$, 3, 4 and 5, and for $d = 0.1$, 1, 10 and 100. Streamlines of the most unstable disturbances are shown as continuous lines and isotherms as dotted lines. In some cases the isotherms are not clearly visible and therefore the vertical component of the temperature disturbance is also shown. The aspect ratio of each set of isolines corresponds precisely to the critical wavenumber.

The description of the onset modes given above may be seen easily in Fig. 3. Most obviously seen is the predominance of the convective motion within the internal porous sublayers with relatively weak flow in the outer sublayers. While this was to be expected when d is small, given the physical arguments above, it is also true when $d = 10$. The above-mentioned fact that the temperature perturbation is 'unicellular' means that the buoyancy force driving convection in the outer sublayers will be the smallest of all the sublayers. In addition, the buoyancy force at any particular value of x (say half way along each of these subfigures in the x-direction) will have the same sign in each sublayer, and therefore the dividing streamline corresponds to flow in the same direction in all the sublayers.

The effect of the conductivity of the solid partition is also clear: there are relatively large temperature drops across the partition when d is small, which is associated with the continuity of heat flux, but they are almost perfectly isothermal when d is large. Thus when $d = 100$, the pertubation temperature profile in each of the partitions is very slightly parabolic with an opposite curvature to that of the profiles in the porous sublayers.

4.2. Mode shapes and critical values for higher modes

In this subsection we concentrate on how the critical values of the Rayleigh number and wavenumber vary with changes in the conductivity ratio, d. Attention is focussed on having very thin solid partitions where $\delta = 10^{-3}$. The qualitative nature of the following comments also apply for other values of δ.

Fig. 4 shows the first four mode shapes for each of the conductivity ratios, $d = 10^{-4}$, $d = 1$ and $d = 10^4$, when the layer consists of $N = 4$ porous sublayers. We note that the vertical component of the disturbance temperature profile, as given by the narrow inset to the right of each set of contours, has $n - 1$ nodal points for mode-n.

When the solid layers have a small conductivity, as represented by $d = 10^{-4}$, convection is essentially confined to the middle two layers for the first two modes. As before, this is due to the fact that each of these sublayers are almost autonomous CHF/CHF layers. The first two modes are distinguished by the fact that cells are corotating for mode 1 but are contrarotating for mode 2. The critical values of the Rayleigh number are, respectively, 14.25596 and 16.07931, which are both relatively close to 12. On the other hand, modes 3 and 4 are concentrated in the outer two sublayers, which are effectively separate CT/CHF systems. The respective critical Rayleigh numbers are 27.52554 and 27.52672, which are very close to one another and are just above the pure single layer CT/CHF value of 27.09762. The closeness of these critical values to one another reflects a large amount of exponential decay in the disturbance profiles across sublayers 2 and 3, and therefore sublayers 1 and 4 are only very slightly coupled to one another. Once more, mode 3 consists of co-rotating cells, while mode 4 has contrarotating cells.

When $d = 1$, the porous and solid sublayers have equal conductivity. Given how thin the solid layers are, they are effective only in preventing flow between porous sublayers; both the temperature and temperature gradient are essentially continuous between the porous sublayers, and this configuration is now very close to that considered in [1]. Graphically, the modes depicted in Fig. 4 are indistinguishable from those corresponding to the configuration of [1]. The critical data themselves are compared in Table 2, below.

When d is large the interfaces act as a CT boundary and therefore Ra_c and k_c are close to that of the classical CT/CT Darcy–Bénard problem. For this extreme case, convection remains strongest in

Table 2
Critical values of Ra and k for the first four modes of the case, $N = 4$, $\delta = 10^{-4}$ and $d = 1$, and a comparison with the results of Rees and Genç [1].

Mode	Present		Rees and Genç [1]	
	Ra_c	k_c	Ra_c	k_c
1	18.73965	1.61159	18.72870	1.61159
2	27.10259	2.32576	27.09763	2.32622
3	35.49088	2.88477	35.49975	2.88534
4	39.44887	3.14042	39.47842	3.14159

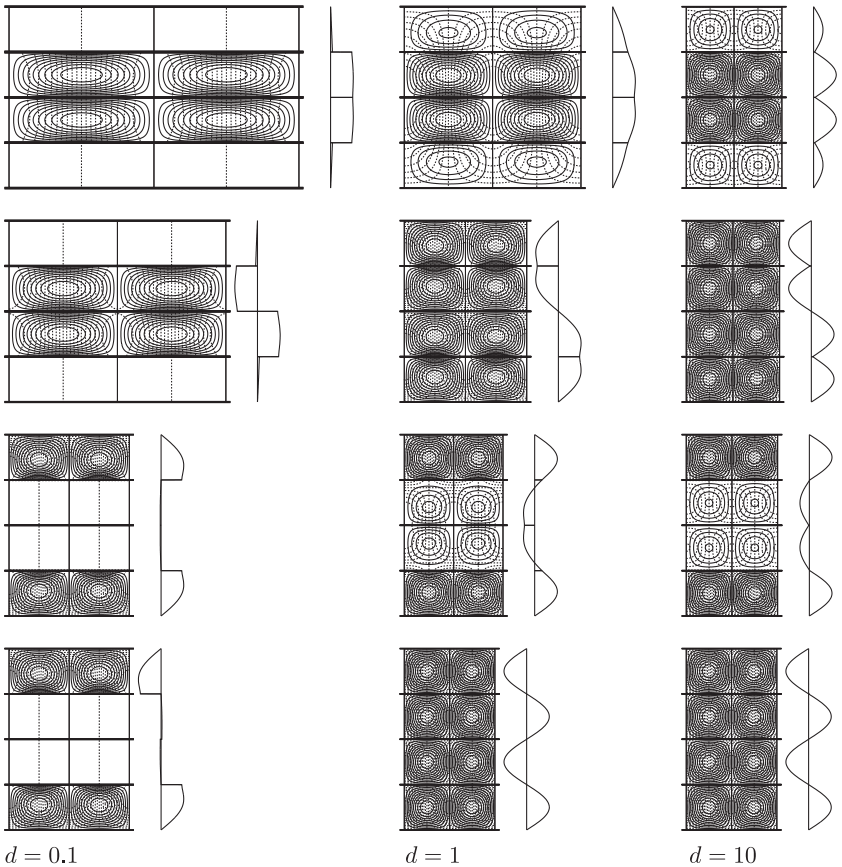

Fig. 4. Profiles of the first four modes for $N = 4$ and $\delta = 0.1$ with $d = 10^{-4}$, 1 and 10^4. Mode 1 corresponds to the uppermost row and mode 4 to the lowest.

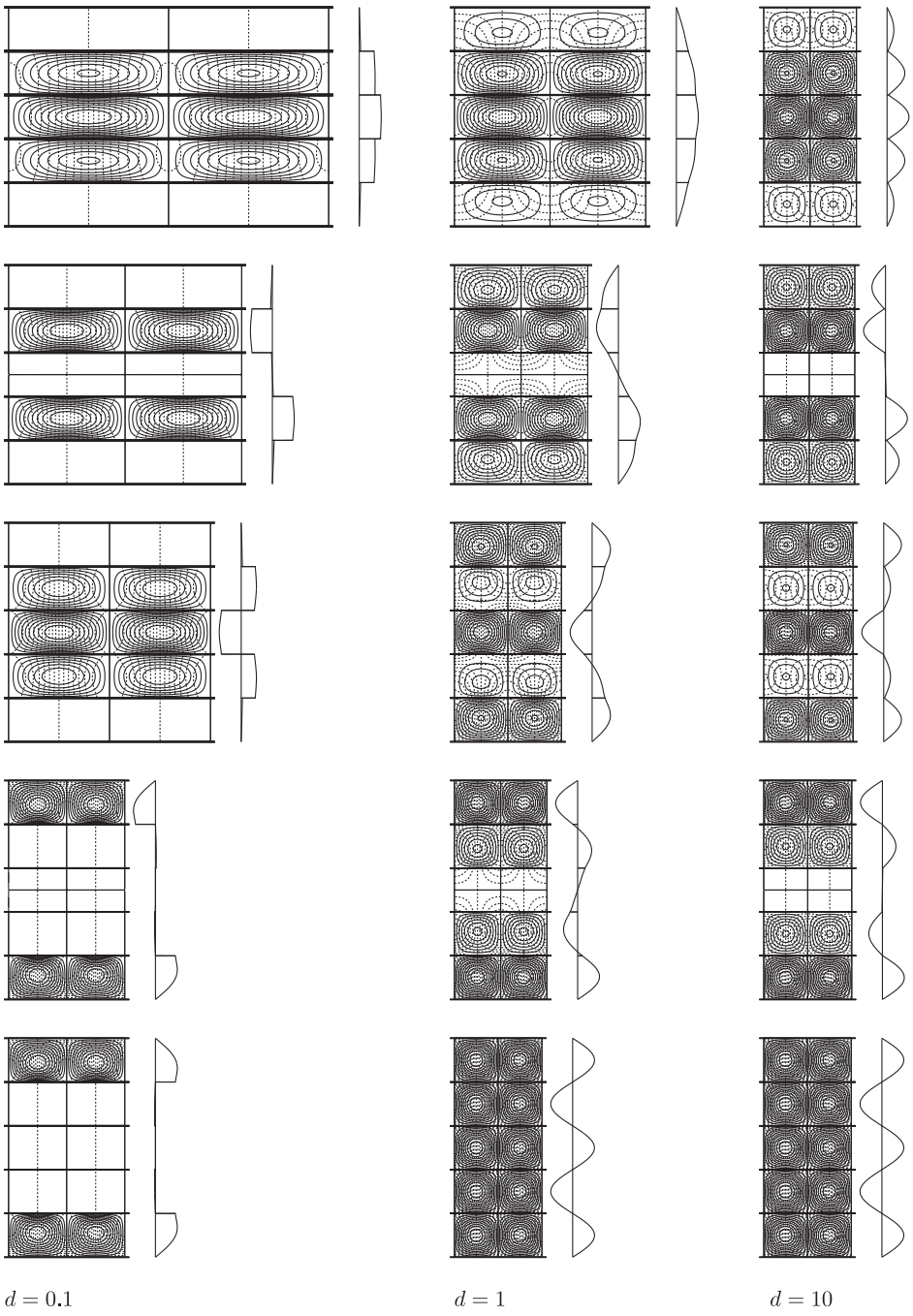

Fig. 5. Profiles of the first five modes for $N = 5$ and $\delta = 0.1$ with $d = 10^{-4}$, 1 and 10^4. Mode 1 corresponds to the uppermost row and mode 5 to the lowest.

Table 3
Critical values of Ra and k for the first five modes of the case, $N = 5$, $\delta = 10^{-4}$ and $d = 1$, and a comparison with the results of Rees and Genç [1].

Mode	Present		Rees and Genç [1]	
	Ra_c	k_c	Ra_c	k_c
1	17.24743	1.43713	17.23633	1.43752
2	23.61044	2.06182	23.60320	2.06231
3	30.63340	2.56866	30.63505	2.56922
4	36.82024	2.97028	36.83562	2.97103
5	39.44691	3.14034	39.47842	3.14159

Table 4
Critical values of Ra and k for the case, $N = 2$, with $d\delta = 0.1$ and 1. Showing the approach to self-similarity as $\delta \to 0$.

δ	$d\delta = 0.1$			$d\delta = 1$		
	d	Ra_c	k_c	d	Ra_c	k_c
10^{-1}	10^{0}	28.21986	2.32410	10^{1}	33.85211	2.54310
10^{-2}	10^{-1}	28.22451	2.32365	10^{0}	33.87078	2.54251
10^{-3}	10^{-2}	28.22456	2.32364	10^{-1}	33.87097	2.54251
10^{-4}	10^{-3}	28.22456	2.32364	10^{-2}	33.87097	2.54251

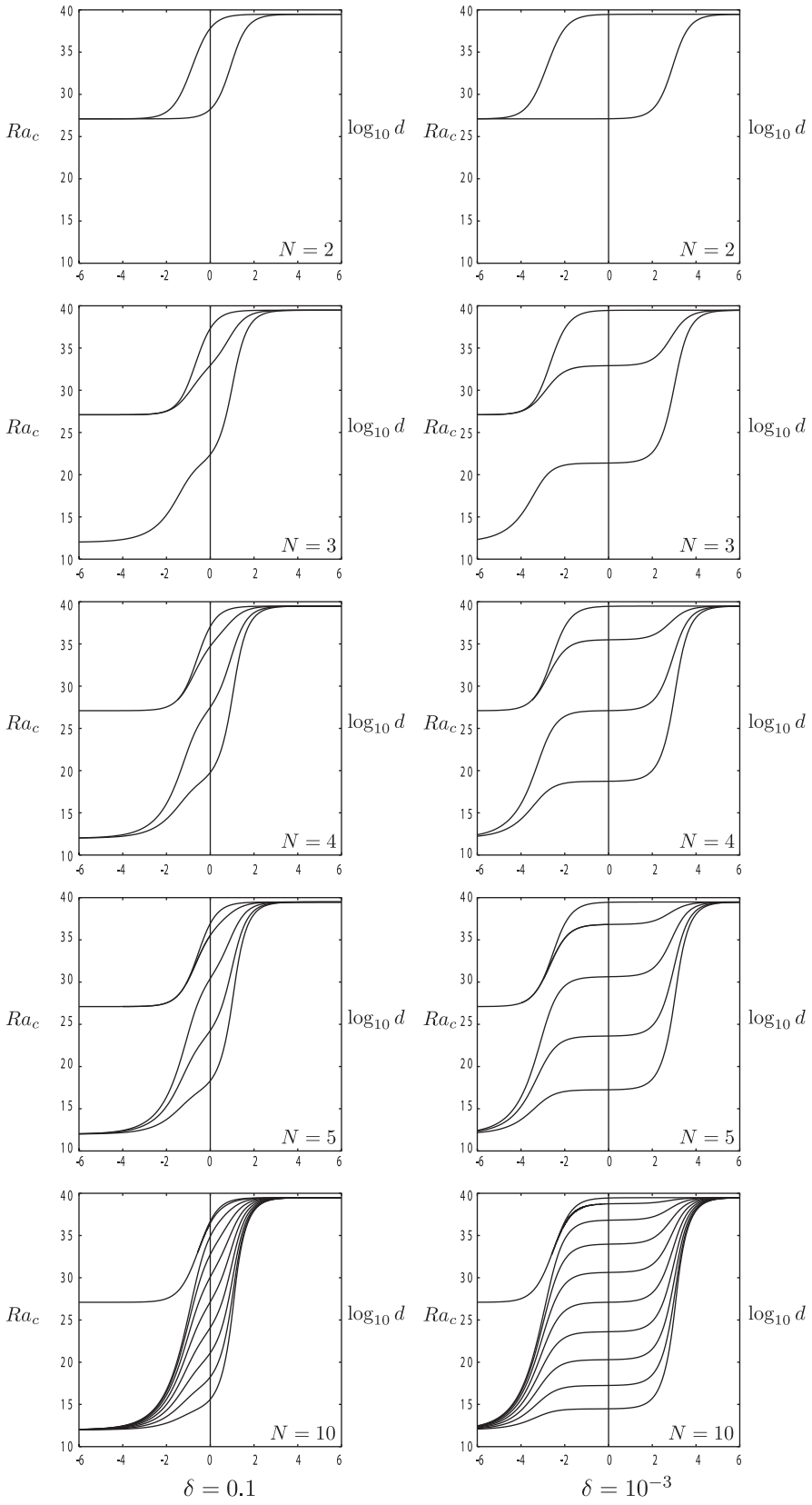

Fig. 6. Variation of Ra_c with d for the first N modes for $N = 2$, 3, 4, 5 and 10, with $\delta = 10^{-1}$ (left) and $\delta = 10^{-3}$ (right).

the middle two layers for mode 1, and cells situated above one another co-rotate. For mode 2, two pairs for co-rotating cells appear, although the upper two rotate in the opposite direction to the lower two. Indeed, for each of the three values of d that have been considered here, the order in which the modes appear when we consider the direction of rotation of the cells remains the same.

Fig. 5 shows the corresponding situation when $N = 5$. The number of nodal points in the vertical disturbance profile remains as

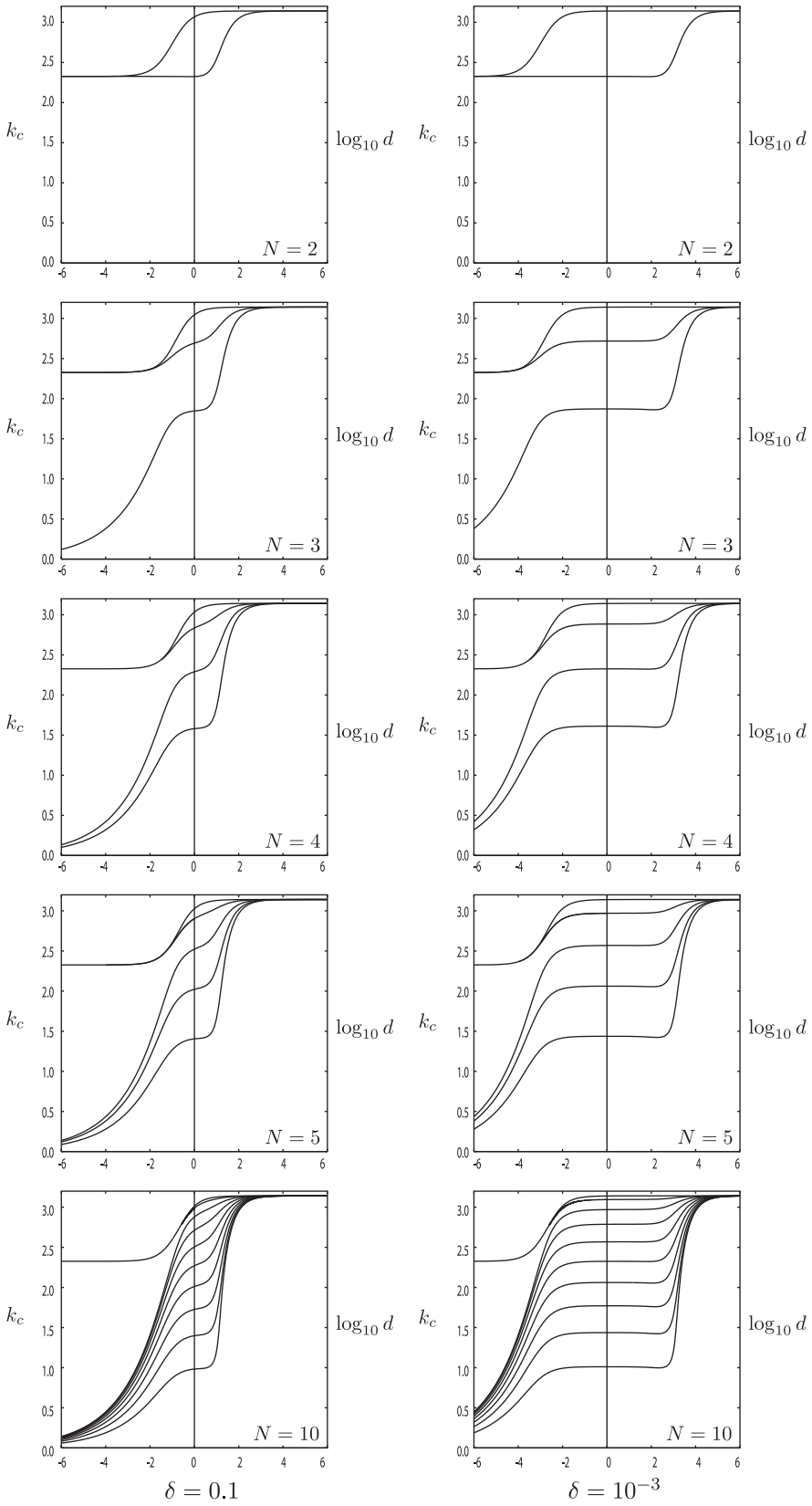

Fig. 7. Variation of k_c with d for the first N modes for $N = 2$, 3, 4, 5 and 10, with $\delta = 10^{-1}$ (left) and $\delta = 10^{-3}$ (right).

$n - 1$ for mode n. Now that there are an odd number of porous sublayers, some of the qualitative features which arose when N is even are modifed when N is odd, while some remain the same. Thus mode 1 still consists of a set of corotating cells stacked above one another in the internal sublayers, and mode N consists of a set of contrarotating cells. On the other hand, modes 2 and 4 each have a very weak pair of contrarotating cells in sublayer 3. The dashed lines which appear in Fig. 5 indicate the temperature

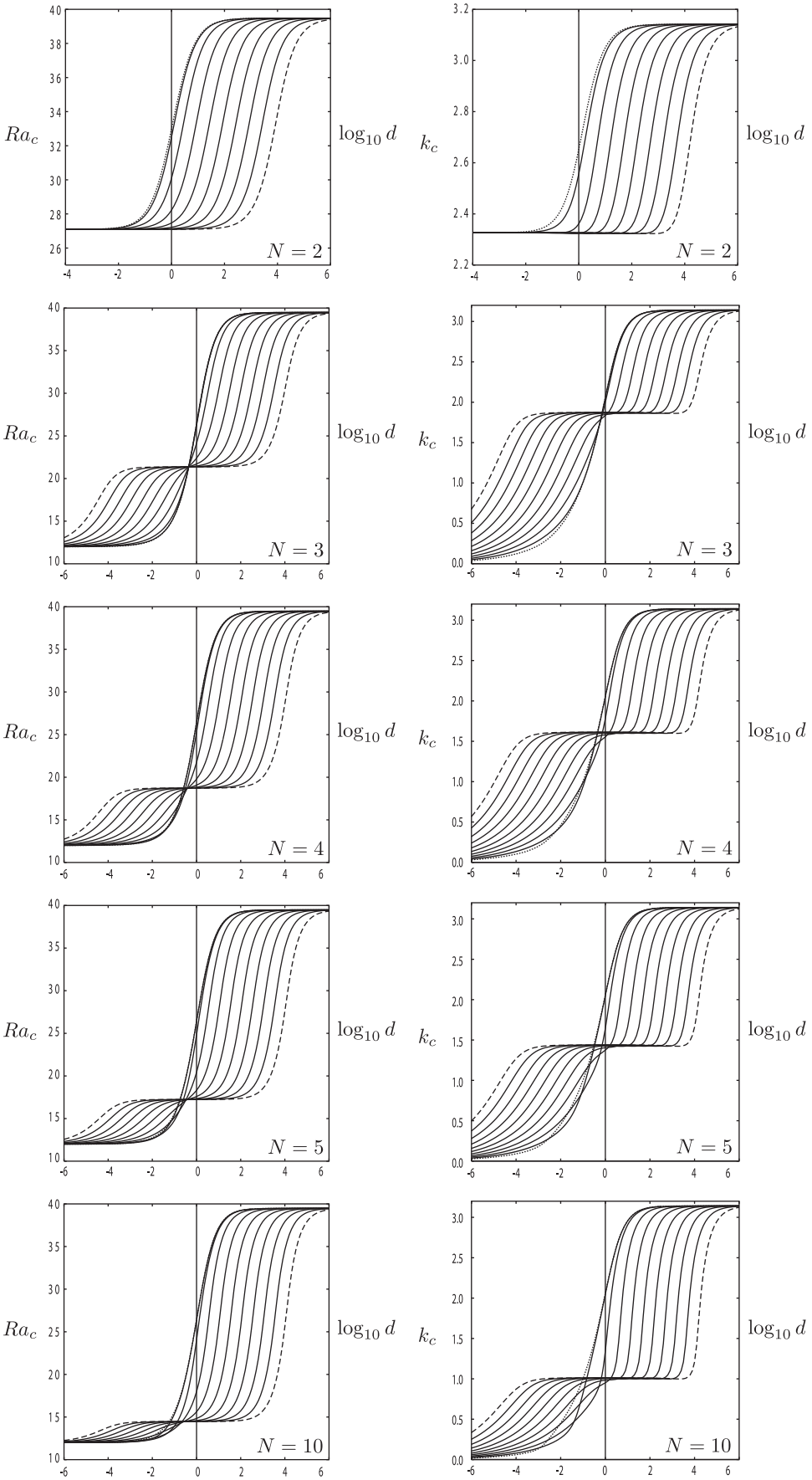

Fig. 8. Variation of Ra_c (left) and k_c (right) with d for the first mode for $N = 2$, 3, 4, 5 and 10, for $\delta = 10^{-4}$ (dashed), $10^{-3.5}$,10^{-3},…,10^{0},$10^{0.5}$ and 10^{1} (dotted).

disturbance, but the continuous line appears half-way up sublayer 3 for modes 2 and 4 is the zero contour for the streamfunction and demonstartes the presence of two weak contrarotating cells.

When $d = 1$, the system reverts once more to that considered in [1], and Table 3 shows how close the two systems are in terms of their critical values (see Table 4).

When $d = 10^4$ all the critical values are close to $Ra_c = 4\pi^2$ and $k_c = \pi$, and this demonstrates that the results of Rees and Genç [1] do not now apply even though the partitions have the very small thickness, $\delta = 10^{-4}$. This indicates that the concept of 'small' with regard to the magnitude of δ depends on the value of d. This may be explained by appealing to Figs. 6 and 7.

Figs. 6 and 7 show how the critical values for the first N modes vary with d. For each of $N = 2, 3, 4, 5$ and 10 this variation is shown for both $\delta = 10^{-1}$ and $\delta = 10^{-3}$ where critical Rayleigh numbers are depicted in Fig. 6 and the corresponding wavenumbers in Fig. 7. Values of d vary from 10^{-6}, which corresponds to very highly insulating solid partitions, to 10^6, which corresponds to very highly conducting solid partitions.

Figs. 6 and 7 show that, for all values of N, there are always two modes (namely, modes $N-1$ and N) for which $Ra_c \to 27.097628$ and $k_c \to 2.326214$ as $d \to 0$. These modes are always concentrated in the outer porous sublayers which are both effectively CT/CHF layers. Convection is then very weak within the internal porous sublayers. We find that mode N always corresponds to contrarotating cells in the outer two sublayers when N is even and to corotating cells when N is odd. Modes 1 to $N-2$ are always concentrated in the internal sublayers, which are effectively CHF/CHF layers, and therefore $Ra_c \to 12$ and $k_c \to 0$ as $d \to 0$. In general, mode 1 consists of corotating cells and mode $N-2$ to contrarotating cells.

At the opposite extreme where $d \to \infty$ all of the porous sublayers are effectively equivalent to CT/CT layers and are therefore very weakly coupled. Hence the critical values obey $Ra_c \to 4\pi^2$ and $k_c \to \pi$ in that limit. For mode 1 convection now takes the form of corotating cells with an amplitude which varies in such a manner that the largest amplitude is half-way up the layer. Mode N consists of otherwise identical contrarotating cells.

When d takes intermediate values the behaviour the critical parameters depends very much on the thickness of the solid partitions. When δ is relatively large, as represented by $\delta = 0.1$ in Figs. 6 and 7, both Ra_c and k_c vary rapidly as d increases through values close to $d = 1$. On the other hand, when δ is very small, such as is represented by $\delta = 10^{-3}$, then there is a very distinct intermediate region centred roughly on $d = 1$ where the critical parameters vary only very slightly with d. This intermediate regime is significant because the values of the critical parameters there are approximately those which were obtained by Rees and Genç [1], where the solid partitions were taken to be infinitesimally thin and where continuity of temperature and heat flux conditions were applied. In the case, $\delta = 10^{-3}$, which is shown in Figs. 6 and 7, it is clear that, despite the thinness of the solid partitions there are ranges of values of d for which that thinness appears to be irrelevant. By this is meant that the critical values for Ra_c and k_c tend towards those of the single CHF/CHF layer when $d \to 0$ and of the CT/CT layer when $d \to \infty$. The curves seem to indicate that the results of [1] are obtained when $10^{-2.5} < d < 10^{2.5}$ when $\delta = 10^{-3}$.

The properties of this intermediate range are shown more clearly in Fig. 8, which shows the variation of the critical values with d for a selection of values of δ and for the same set of values of N. This figure may be regarded as being the closest that one might reasonably get to a summary of the onset criteria for the general problem of a porous layer with the type of sublayers we are considering.

For $N = 2$ there is no intermediate regime, but simply a smooth transition from the small-d limit to the large-d limit. However, a comparison of the critical data for different values of δ when *delta* is small, suggests that critical values are a function of $d\delta$ when $d \gg 1$. This may be seen very clearly in the following Table, which gives the critical data for the case $N = 2$ and for $d\delta = 0.1$ and $d\delta = 1$.

For $N = 2$, the critical values corresponding to the limit, $\delta \to \infty$, are achieved to a high degree of accuracy well before δ rises to $\delta = 10$, which is depicted as a dotted line in Fig. 8. For such a thick solid partition the temperature field decays with e-folding distance $1/k$, given the form of Eq. (18). Here we have $k \simeq 2.326$, and therefore the temperature field in the bulk of the solid partition varies only by exponentially small amounts when $\delta = 10$.

When there are three or more porous sublayers, then the critical values (both Ra_c and k_c) exhibit a very distinctive but universal variation as d increases from very small values to very large values when the partitions are thin. When $d \ll 1$ then $Ra_c \sim 12$ and $k_c \sim 0$. When d rises to just above the value of δ, there is a rapid transition towards a regime in which the system is well-modelled by the analysis of Rees and Genç [1]. A second transition takes place close to $d = \delta^{-1}$ and the critical values then tend towards a final steady regime in which $Ra_c \sim 4\pi^2$ and $k_c \sim \pi$. Therefore these properties suggest the general observation that critical values found in [1] for which $\delta = 0$, are valid to a high degree of accuracy for small values of δ, but only when

$$10^{-\gamma+0.5} < d < 10^{\gamma-0.5}, \tag{34}$$

where $\delta = 10^{-\gamma}$, and where $\gamma > 1$. Thus, for $\delta = 10^{-1}$ we require that $10^{-0.5} < d < 10^{0.5}$, and this represents the largest value of δ for which (34) holds.

When $N \geqslant 3$, we may summarise as follows. We may say that if d is fixed, then the critical values found in [1] are obtained as $\delta \to$, which is intuitive. Conversely, if δ is fixed (even if this is an extremely small value), then $d \to \infty$ recovers the critical values corresponding to the CT/CT single layer, while $d \to 0$ yields those corresponding to the CHF/CHF layer. However, a form of self-similarity exists if we allow both d and δ to vary in a manner in which they are linked. If either $d\delta$ or d/δ remain constant as $\delta \to 0$, then the critical values depend on those respective constants.

5. Conclusions

The aim of this paper has been to present a comprehensive physical understanding of the behaviour of the critical parameters (Ra_c and k_c) as functions of the governing parameters, d, δ and N, and to give some explanations in terms of the profiles of the onset modes. The linear stability analysis used a computed dispersion relation in order to determine the neutral curves and the associated mode shapes. Our results have been set into the context of the work by Rees and Genç [1] who considered the zero-partition-thickness limit, $\delta = 0$. In that paper, it was assumed that there was continuity of heat flux across the zero-thickness partitions, and therefore it was deemed that the conductivity of those partitions played no role. In the present paper we have considered partitions of finite thickness, but have found that the results of Rees and Genç [1] also apply when δ is very small, but that there is a restriction on the allowable range of values of the conductivity ratio, d, for which this remains true. Thus, for a fixed value of d, whatever its magnitude, the results of [1] will eventually be attained as $\delta \to 0$, but if either $d\delta$ or d/δ is allowed to remain constant as $\delta \to 0$ the resulting critical values will depend on the magnitude of the constant.

Modal shapes were found to be concentrated within the interior sublayers independently of the values of the governing parameters. In some cases the magnitude of the disturbances in the outer sublayers is only slightly smaller than those in the interior sublayers; generally this happens when d is large or δ is small, but this conclusion depends on the relative magnitudes of these parameters. In

other cases there is almost no disturbance in the outermost sublayers.

Many of the results presented here rely heavily on the symmetries of the composite layer which is composed of identical porous sublayers and identical solid partitions. Generally, an imperfection in any of the sublayers (such as the thickness or conductivity) or a solid partition, will destroy the symmetries which have been found in the modal profiles. This might open the way for the production of more exotically-shaped neutral curves.

Acknowledgements

The first-named author (PMP) wishes to thank the Commonwealth Scholarship Commission at the Association of Commonwealth Universities, London, UK, for funding a Commonwealth Academic Fellowship at the University of Bath. He also wishes to thank the University of Bath for providing the facilities to enable the research presented in this paper. Finally, he wishes to thank the Management and Principal of JSS College, Dharwad, India, for granting leave to travel to the UK.

References

[1] D.A.S. Rees, G. Genç, The onset of convection in porous layers with multiple horizontal partitions, Int. J. Heat Mass Transfer 54 (2011) 3081–3089.
[2] M.R.E. Proctor, C.A. Jones, The interaction of two spatially resonant patterns in thermal convection. Part 1. Exact 1:2 resonance, J. Fluid Mech. 188 (1988) 301–335.
[3] I. Catton, J.H. Lienhard V, Thermal stability of two fluid layers separated by a solid interlayer of finite thickness and thermal conductivity, ASME J. Heat Transfer 106 (1984) 13–17.
[4] R. McKibbin, M.J. O'Sullivan, Onset of convection in a layered porous medium heated from below, J. Fluid Mech. 96 (1980) 375–393.
[5] R. McKibbin, M.J. O'Sullivan, Heat transfer in a layered porous medium heated from below, J. Fluid Mech. 111 (1981) 141–173.
[6] R. McKibbin, P.A. Tyvand, Anisotropic modelling of thermal convection in multilayered porous media, J. Fluid Mech. 118 (1982) 315–339.
[7] R. McKibbin, P.A. Tyvand, Thermal convection in a porous medium composed of alternating thick and thin layers, Int. J. Heat Mass Transfer 26 (1983) 761–780.
[8] R. McKibbin, P.A. Tyvand, Thermal convection in a porous medium with horizontal cracks, Int. J. Heat Mass Transfer 27 (1984) 1007–1023.
[9] T. Masuoka, T. Katsuhara, Y. Nakazono, S. Isozaki, Onset of convection and flow patterns in a porous layer of two different media, Heat Transfer Jpn. Res. 7 (1979) 39–52.
[10] R. Rana, R.N. Horne, P. Cheng, Natural convection in a multi-layered geothermal reservoir, Trans. ASME C J. Heat Transfer 101 (1979) 411–416.
[11] D.A.S. Rees, D.S. Riley, The three-dimensional stability of finite-amplitude convection in a layered porous medium heated from below, J. Fluid Mech. 211 (1990) 437–461.
[12] J.Y. Jang, W.L. Tsai, Thermal instability of two horizontal porous layers with a conductive partition, Int. J. Heat Mass Transfer 31 (1988) 993–1003.
[13] D.A. Nield, A. Bejan, Convection in Porous Media, 4th ed., Springer-Verlag, New York, 2013.
[14] D.A.S. Rees, A. Mojtabi, The effect of conducting boundaries on weakly nonlinear Darcy–Bénard convection, Transp. Porous Media 88 (2011) 45–63.